

# Quantum Breakdown Condensate as a Disorder-Free Quantum Glass

Yu-Min Hu,<sup>1</sup> Zhaoyu Han,<sup>2,\*</sup> and Biao Lian<sup>3,†</sup>

<sup>1</sup>*Max Planck Institute for the Physics of Complex Systems, Nöthnitzer Straße 38, 01187 Dresden, Germany*

<sup>2</sup>*Department of Physics, Harvard University, Cambridge, Massachusetts 02138, USA*

<sup>3</sup>*Department of Physics, Princeton University, Princeton, New Jersey 08544, USA*

We study the phase diagram of a one-dimensional spin quantum breakdown model, which has an exponential  $U(1)$  symmetry with charge unit decaying as  $2^{-j}$  with site position  $j$ . By exact diagonalization (ED), we show that the model with spin  $S \geq 2$  exhibits an exponential  $U(1)$  spontaneous symmetry breaking (SSB) phase dubbed a quantum breakdown condensate. It exhibits a bulk gap violating the Goldstone theorem, and an edge mode only on the left edge if in open boundary condition. In a length  $L$  lattice, the condensate has  $\mathcal{O}(2^L)$  number of SSB ground states originating from the  $\mathcal{O}(2^L)$  number of exponential  $U(1)$  charge sectors, leading to a finite entropy density  $\ln 2$ . This enforces a first order SSB phase transition into this phase, as observed in ED and verified in the large  $S$  limit on an exactly solvable Rokhsar-Kivelson line. The condensate has an SSB order parameter being the local in-plane spin, which points in angles related by the chaotic Bernoulli (dyadic) map and thus is effectively random. Moreover, we show the condensate exhibits non-decaying local autocorrelations, and does not have an off-diagonal long-range order. The quantum breakdown condensate thus behaves as a disorder-free quantum glass and is beyond the existing classifications of phases of matter.

Symmetries and spontaneous symmetry breaking (SSB) play a unifying role in the classification and characterization of quantum phases of matter. Recently, generalized symmetries [1, 2] have attracted extensive interests, examples including dipole [3–11], multipole [12, 13], subsystem symmetries [14–21], and more recently exponential symmetries [22–32]. On lattices, a class of on-site symmetries is the modulated symmetry with symmetry charge  $\hat{Q} = \sum_j f_j \hat{n}_j$ , where the unit of charge  $f_j$  depends on site  $j$ , and  $\hat{n}_j$  is the particle number. For instance, in one dimension (1D), the  $k$ -th multipole  $U(1)$  symmetry has  $f_j = j^k$ , and the exponential  $U(1)$  symmetry with base  $q \neq 1$  has  $f_j = f_0 q^{-j}$ , for which translationally invariant models can be written down.

Particularly, as found in a recent mean-field study [25], the SSB ground state of a boson quantum breakdown model with exponential  $U(1)$  symmetry, dubbed the quantum breakdown condensate, exhibits a gapped excitation spectrum violating the Goldstone theorem. This motivates us to uncover more unconventional characters of this state, and to explore its realization in more generic models.

In this letter, we propose and study the SSB of a 1D spin quantum breakdown model [Eq. (1)], which has an exponential  $U(1)$  symmetry with base  $q = 2$ . Compared to the boson model [25], the spin model has a finite on-site Hilbert space and is more experimentally feasible. Employing exact diagonalization (ED), we find the model with spin  $S \geq 2$  generically undergoes a phase transition from a symmetric paramagnetic (PM) phase to the exponential  $U(1)$  SSB quantum breakdown condensate. We verify that the condensate has a bulk gap as found in [25], and we further reveal an edge mode only existing on the left edge which alters the ED spectrum for open boundary condition. For a lattice of length  $L$ , we find

the condensate has  $\mathcal{O}(2^L)$  SSB ground states originating from  $\mathcal{O}(2^L)$  number of charge sectors, which span a finite total bandwidth, in contrast to typical SSB. Also, both [25] and our ED here find the SSB phase transition being first order. We further identify a Rokhsar-Kivelson line in the large  $S$  limit to be an exactly solvable first order phase boundary. We argue that this SSB phase transition has to be first order, as enforced by a finite entropy density  $\ln 2$  from  $\mathcal{O}(2^L)$  ground states in the condensate. Moreover, we show the condensate has a local SSB order parameter giving in-plane spins pointing in angles related by the chaotic Bernoulli (dyadic) map [33] from site to site, which typically look random. We also find it exhibits non-decaying local autocorrelations, and has no off-diagonal long range order. These facts indicate the quantum breakdown condensate behaves as a disorder-free quantum glass, and lies beyond any known classifications of phases of matter.

*The model.* In a spin chain of length  $L$  with a spin  $S \geq 1$  at each site, we define the 1D spin quantum breakdown model Hamiltonian [Fig. 1(a)]:

$$\hat{H} = -\frac{J}{(2S)^{3/2}} \sum_{j=1}^{L_{P \setminus O}} \left[ \hat{S}_j^- (\hat{S}_{j+1}^+)^2 + \hat{S}_j^+ (\hat{S}_{j+1}^-)^2 \right] - h \sum_{j=1}^L \left[ \lambda \hat{S}_j^z + (1-\lambda) \frac{4S^2}{\pi^2} \sin \left( \frac{\pi}{2S} \hat{S}_j^z \right) \right], \quad (1)$$

where  $\hat{S}_j^\nu$  ( $\nu = x, y, z$ ) are the spin operators on site  $j$ , and  $\hat{S}_j^\pm = \hat{S}_j^x \pm i \hat{S}_j^y$ . The first term with coefficient  $-J/(2S)^{3/2}$  is the inversion asymmetric breakdown interaction [22], in which the sum is up to  $L_O = L - 1$  for open boundary condition (OBC), and up to  $L_P = L$  for periodic boundary condition (PBC) with site  $L + j$  identified with site  $j$ . The second term is a nonlinear

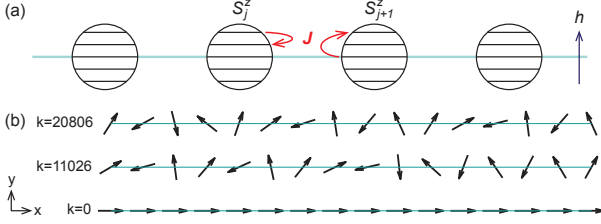


FIG. 1. (a) Illustration of the spin breakdown model in Eq. (1). (b) The in-plane spin directions on different sites for the quantum breakdown condensate under PBC with order parameter  $\langle S_j^+ \rangle = \alpha_S e^{i2^{L-j}\theta}$ . We take  $L = 16$  and  $\theta = \frac{2\pi}{2^L-1}k$  with representative  $k$  values labeled in the plot.

coupling to a  $z$ -direction magnetic field  $h$  with  $\lambda \in [0, 1]$ , which reduces to linear when  $\lambda = 1$ .

The model in Eq. (1) has an exponential symmetry  $\hat{U}(\varphi) = \exp(i\varphi \sum_{j=1}^L 2^{L-j} \hat{S}_j^z)$ , which transforms the spin on site  $j$  as  $\hat{U}(\varphi)(\hat{S}_j^z, \hat{S}_j^\pm)\hat{U}(\varphi)^\dagger = (\hat{S}_j^z, e^{\pm i2^{L-j}\varphi} \hat{S}_j^\pm)$ . For OBC, any angle  $\varphi \in [0, 2\pi)$  is allowed, which gives a  $U(1)$  exponential symmetry. For PBC, the transformation on site  $j = L$  should be identical to  $j = 0$ , which enforces  $(2^L-1)\varphi = 0 \pmod{2\pi}$ , leading to a reduction from  $U(1)$  to  $\mathbb{Z}_{2^L-1}$  exponential symmetry depending on system size  $L$ . We can rewrite  $\hat{U}(\varphi) = e^{i\varphi \hat{Q}}$  as generated by an exponential charge  $\hat{Q}$ :

$$\hat{Q} = \begin{cases} \sum_{j=1}^L 2^{L-j} \hat{S}_j^z, & (\text{OBC}) \\ \sum_{j=1}^L 2^{L-j} \hat{S}_j^z \pmod{2^L-1}. & (\text{PBC}) \end{cases} \quad (2)$$

The number of charge sectors is  $N_Q = 2S(2^L-1) + 1$  for OBC, and  $N_Q = 2^L-1$  for PBC, respectively. As  $L \rightarrow \infty$ , we shall simply call  $\hat{U}(\varphi)$  an exponential  $U(1)$  symmetry regardless of boundary conditions. For PBC, there is additionally a translation symmetry  $\hat{T}$  sending site  $j$  to  $j+1$ , which does not commute with the exponential symmetry:  $\hat{T}\hat{U}(\varphi)\hat{T}^{-1} = \hat{U}(2\varphi)$ .

*Large spin limit and RK line.* We first analyze the phases of the model in the large spin limit. For  $h > 0$ , by a Holstein-Primakoff transformation  $\hat{S}_j^z = S - \hat{n}_j$ ,  $\hat{S}_j^+ = (\hat{S}_j^-)^\dagger = \sqrt{2S - \hat{n}_j} \hat{a}_j$  with boson operators  $\hat{a}_j, \hat{a}_j^\dagger$  and  $\hat{n}_j = \hat{a}_j^\dagger \hat{a}_j$ , and taking  $S \rightarrow \infty$ , one can map the spin model in Eq. (1) to the boson quantum breakdown model [25]:

$$\begin{aligned} \hat{H} = & -J \sum_{j=1}^{L_{P\setminus O}} \left[ \hat{a}_j (\hat{a}_{j+1}^\dagger)^2 + \hat{a}_j^\dagger (\hat{a}_{j+1})^2 \right] \\ & + \sum_{j=1}^L \left[ -\mu \hat{n}_j + \frac{U}{2} \hat{n}_j (\hat{n}_j - 1) \right], \end{aligned} \quad (3)$$

with a Hubbard interaction  $U = (1 - \lambda)h$  and chemical potential  $\mu = -(1 + \lambda)h/2$ . As numerically revealed in [25], as  $J/U$  increases, the ground state of boson model

in Eq. (3) undergoes a phase transition from a symmetric *Mott insulator* to a *quantum breakdown condensate* with the exponential symmetry spontaneously broken.

Here we present an analytical understanding for this spontaneous symmetry breaking (SSB) near a Rokhsar-Kivelson (RK) line, which is defined by  $\mu U = -2J^2$  with  $U > 0$ . On this RK line, by defining a real parameter  $\alpha = 2J/U$ , we can rewrite the boson Hamiltonian  $H$  in Eq. (3) (exactly for PBC, and up to boundary terms for OBC) into a semi-positive definite form:

$$\hat{H}_{\text{RK}} = \frac{U}{2} \sum_j \hat{O}_j^\dagger \hat{O}_j, \quad \hat{O}_j = \hat{a}_{j+1}^2 - \alpha \hat{a}_j. \quad (4)$$

Apparently, a state  $|\Psi\rangle$  satisfying  $\hat{O}_j|\Psi\rangle = 0$  for all  $j$  gives an exact ground state of  $H_{\text{RK}}$  with energy  $E_{\text{gs}} = 0$ , which has two families of solutions (unnormalized):

$$|\Psi_{\text{sym}}\rangle = |0\rangle, \quad |\Psi_{\text{ssb}}(\theta)\rangle = \prod_{j=1}^L \exp(\alpha e^{i2^{L-j}\theta} \hat{a}_j^\dagger) |0\rangle, \quad (5)$$

where  $\theta \in 2\pi\mathbb{R}/\mathbb{Z}$  for OBC, and  $\theta \in \frac{2\pi}{2^L-1}\mathbb{Z}_{2^L-1}$  for PBC, while  $|0\rangle$  is the boson vacuum. Thus,  $H_{\text{RK}}$  in Eq. (4) is a frustration free Hamiltonian with solvable ground states in Eq. (5) [34, 35].  $|\Psi_{\text{sym}}\rangle$  is a symmetric Mott insulator state with zero boson per site. The coherent state  $|\Psi_{\text{ssb}}(\theta)\rangle$  gives an SSB quantum breakdown condensate, which has a local order parameter  $\langle \hat{a}_j \rangle = \alpha e^{i2^{L-j}\theta}$  breaking the exponential  $U(1)$  or  $\mathbb{Z}_{2^L-1}$  symmetry [25]. The coherent states  $|\Psi_{\text{ssb}}(\theta)\rangle$  can be further superposed into the charge  $Q$  eigenbasis, which gives exactly one ground state  $|\Psi_Q\rangle$  per charge  $Q$  sector.

Similar to the RK model [34, 35], the fact that both  $|\Psi_{\text{sym}}\rangle$  and  $|\Psi_{\text{ssb}}(\theta)\rangle$  are ground states of  $H_{\text{RK}}$  implies that the RK line  $\mu U = -2J^2$  is the phase boundary of the zero-temperature SSB transition. When  $J$  is perturbatively increased (decreased) away from the RK line, the state  $|\Psi_{\text{ssb}}(\theta)\rangle$  ( $|\Psi_{\text{sym}}\rangle$ ) will have a lower energy, leading to the SSB (symmetric) phase. This is an energy level crossing transition with the order parameter  $|\langle \hat{a}_j \rangle|$  jumping discontinuously from 0 to  $|\alpha|$ , which indicates that the RK line is a *first order* phase boundary. This quantitatively matches the numerical results in [25]. In fact, we will argue later that the SSB phase transition of exponential  $U(1)$  symmetry is generically *first order*.

In the spin picture, the SSB order parameter  $\langle \hat{a}_j \rangle$  becomes  $\langle \hat{S}_j^+ \rangle = \alpha_S e^{i2^{L-j}\theta}$ , with  $\alpha_S \neq 0$ . Interestingly, this points the in-plane spin components  $(\langle \hat{S}_j^x \rangle, \langle \hat{S}_j^y \rangle)$  on site  $j$  in an angle  $\theta_j = 2^{L-j}\theta \pmod{2\pi}$ , which is typically a random looking glass-like configuration for generic  $\theta$  [Fig. 1(b)]. In fact, the angles follow a recursion relation  $\theta_j = 2\theta_{j+1} \pmod{2\pi}$ , which is exactly the ergodic and chaotic Bernoulli (dyadic) map [33] describing the Lorenz strange attractor [36–38]. The SSB state is thus analogous to a spin glass, with more evidences to be shown later.

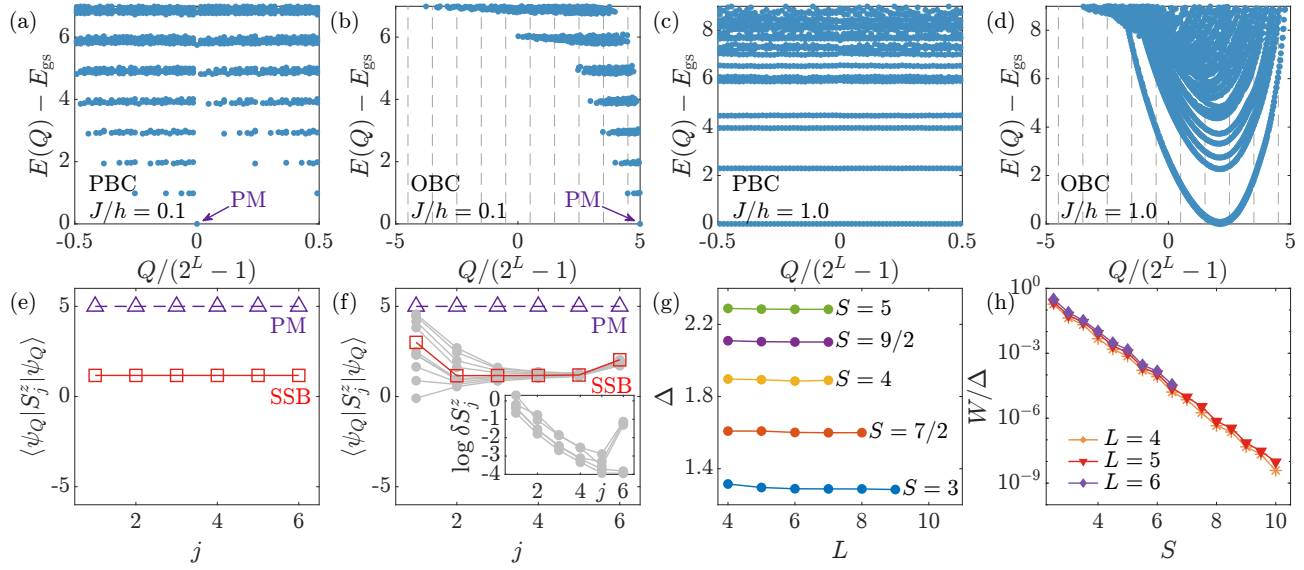


FIG. 2. ED calculations for  $\lambda = h = 1$ . (a-d) The ED spectra (subtracting the global ground state energy  $E_{\text{gs}}$ ) versus charge sector  $Q$  for  $S = 5$ ,  $L = 6$ , in the PM phase ( $J = 0.1$ ) in (a-b) and the SSB quantum breakdown condensate phase ( $J = 1$ ) in (c-d). (a) and (c) are calculated with PBC, (b) and (d) are calculated with OBC. (e-f) The expectation  $\langle \hat{S}_j^z \rangle$  versus site  $j$  for the PM ground state (triangle markers) and the SSB global ground state (square markers), calculated (e) with PBC (for parameters in (a) and (c)), and (f) with OBC (for parameters in (b) and (d)). Dot markers in (f) show  $\langle \hat{S}_j^z \rangle$  of the OBC SSB ground state  $|\psi_Q\rangle$  in charge sectors  $Q \neq Q_0$ , where  $Q_0$  is the charge sector of the global SSB ground state; the (f) inset shows  $\delta S_j^z \equiv \langle \psi_Q | \hat{S}_j^z | \psi_Q \rangle - \langle \psi_{Q_0} | \hat{S}_j^z | \psi_{Q_0} \rangle$  decays exponentially in  $j$ . (g) The excitation gap  $\Delta$  and (h) bandwidth  $W$  of the SSB ground-state manifold with PBC for different  $S$  and  $L$ , where we fix  $J = h = \lambda = 1$ .

*Finite spin.* For finite spin  $S$ , we study the Hamiltonian in Eq. (1) employing exact diagonalization (ED). We find the SSB phase transition of exponential  $U(1)$  symmetry robustly occurs for  $S \geq 2$ , with characters qualitatively agreeing with the above large  $S$  limit analysis. Hereafter, we set  $\lambda = 1$ ,  $h = 1$ , and focus on the example of  $S = 5$ , for which the ground state SSB phase transition happens at  $J = J_0 \approx 0.52$ . The results for other  $S$  are similar (see supplementary material (SM) [39]).

For  $J < J_0$ , the model is in the symmetric phase, denoted as the *paramagnetic* (PM) phase in the spin picture. Fig. 2(a) and (b) show the ED spectra at  $J = 0.1$  for  $L = 6$  with PBC and OBC, respectively, with the horizontal axis labeling the charge sector. The PBC and OBC spectra both have a unique gapped PM ground state, and are similar especially that the PBC charge sectors can be viewed as the OBC charge sectors folded into the range  $Q/(2^L - 1) \in [-1/2, 1/2]$  (folding boundaries marked by dashed lines in Fig. 2(b)). As shown by the triangle marker line in Fig. 2(e)-(f), the PM ground state has spin  $\langle \hat{S}_j^z \rangle = S$  maximally polarized.

In contrast, the ED spectra for  $J > J_0$  in the SSB quantum breakdown phase are notably different between PBC and OBC, as shown in Fig. 2(c) and (d) calculated at  $J = 1$  for  $L = 6$ . For PBC, each charge  $Q$  sector contributes a ground state, the energy of which we denote as  $E_{\text{gs}}(Q)$ . These  $2^L - 1$  states form a nearly degenerate SSB ground state manifold spanning an en-

ergy bandwidth  $W = \max_Q [E_{\text{gs}}(Q)] - \min_Q [E_{\text{gs}}(Q)]$ , and are separated with higher energy states by a finite gap  $\Delta = \min_Q [E_{\text{ex}}(Q)] - \max_Q [E_{\text{gs}}(Q)]$ , where  $E_{\text{ex}}(Q)$  is the lowest excited state energy in charge  $Q$  sector. Fig. 2(g) shows the gap  $\Delta$  is stably finite as  $L$  increases. Fig. 2(h) implies that  $W$  decays exponentially in  $S$ , but is nearly  $L$  independent (bounded by  $W < \Delta$ ). For OBC, as Fig. 2(d) shows, while each charge sector  $Q$  still has a gap (roughly equals to the PBC gap  $\Delta$ ), the full spectrum is gapless. The ground state energy  $E_{\text{gs}}(Q)$  of charge sector  $Q$  is well fitted by  $E_{\text{gs}}(Q) - E_{\text{gs}}(Q_0) \approx D \left( \frac{Q - Q_0}{2^L} \right)^2$  with  $D$  independent of  $L$ , where  $Q_0$  is the charge sector of the global ground state.

To understand the unconventional ED energy spectra of the SSB quantum breakdown condensate, we first note that it has no gapless Goldstone modes as shown by [25]. To see this, consider perturbing the SSB order parameter into  $\langle \hat{S}_j^+ \rangle = \alpha_S e^{i2^{L-j}\theta} e^{i\delta\theta_j}$  with a small phase  $\delta\theta_j$ , which yields a Goldstone boson Lagrangian  $\mathcal{L} = \frac{g_0}{2} \sum_j [(\partial_t \delta\theta_j)^2 - m_b^2 (\delta\theta_j - 2\delta\theta_{j+1})^2]$  as enforced by the symmetry. In the bulk, it can be rewritten as  $\mathcal{L} = \frac{g_0}{2} \sum_j [(\partial_t \delta\theta_j)^2 - 2m_b^2 (\delta\theta_j - \delta\theta_{j+1})^2 - m_b^2 \delta\theta_j^2] \approx \frac{g_0}{2} \int dx [(\partial_t \delta\theta)^2 - v_b^2 (\partial_x \delta\theta)^2 - m_b^2 \delta\theta^2]$ , which gives a bulk gap  $m_b$  matching well with the ED gap  $\Delta$  in Fig. 2(g). For OBC, there is an extra left-edge boson zero mode with  $\delta\theta_j = 2^{-j} \delta\theta_{\text{edge}}$  [25], which simply generates the exponential  $U(1)$  transformation  $e^{i2^{-L} \delta\theta_{\text{edge}} \hat{Q}}$ . Upon quan-

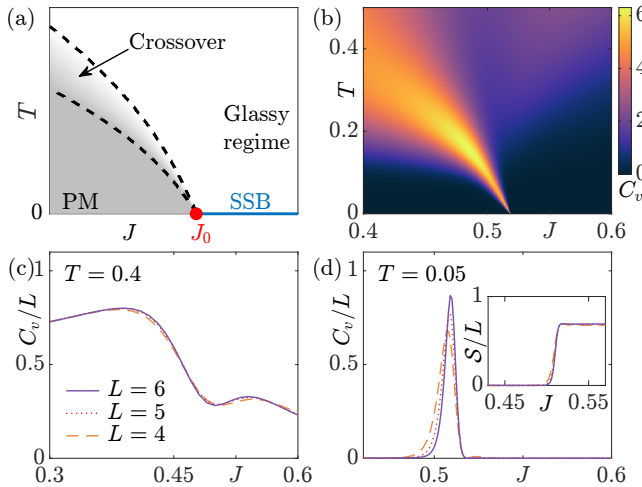


FIG. 3. (a) The phase diagram for Gibbs states. (b) The heat capacity  $C_v$  for  $\lambda = h = 1$ ,  $S = 5$ ,  $L = 6$  with PBC. (c-d) The specific heat  $C_v/L$  versus  $J$  at temperature (c)  $T = 0.4$  and (d)  $T = 0.05$ , for parameters in (b). The inset of (d) shows the entropy density  $S/L$  at  $T = 0.05$ . The legend in (c) labels  $L$  for (c-d).

izing  $\delta\theta_{\text{edge}}$ , this gives a canonical commutation relation  $[\delta\hat{\theta}_{\text{edge}}, 2^{-L}\hat{Q}] = i$ , which indicates  $\partial_t\delta\hat{\theta}_{\text{edge}} \propto \frac{\hat{Q}-Q_0}{2^L}$  with some number  $Q_0$ . The Lagrangian  $\mathcal{L}$  then yields an edge mode Hamiltonian  $\mathcal{H}_{\text{edge}} \propto \frac{q_0}{2}(\partial_t\delta\hat{\theta}_{\text{edge}})^2 \propto \left(\frac{\hat{Q}-Q_0}{2^L}\right)^2$ , which exactly accounts for the ground state energy difference  $E_{\text{gs}}(Q) - E_{\text{gs}}(Q_0)$  in the OBC spectrum in Fig. 2(d). This edge mode can be further seen in Fig. 2(e)-(f). For PBC shown in Fig. 2(e), the ground state  $\langle \hat{S}_j^z \rangle$  of every charge sector is spatially uniform (the line with square markers). For OBC shown in Fig. 2(f), the ground state  $\langle \hat{S}_j^z \rangle$  of generic charge  $Q$  sectors (lines with solid circle markers) differs from that of the charge  $Q_0$  sector (square markers) near site 1, and their differences  $\delta S_j^z$  decay exponentially with site  $j$  (Fig. 2(f) inset), indicating an edge mode. Thus, for OBC, the bulk spectrum is still gapped. We note that the sensitivity of energy spectrum and  $\delta S_j^z$  to boundary conditions is interestingly akin to the skin effect of non-Hermitian systems [40–43].

*Phase diagram.* Since the SSB quantum breakdown condensate at  $J > J_0$  has a bulk gap  $\Delta > 0$  above the ground state manifold, the Mermin-Wagner theorem [44, 45] does not apply, and the SSB is stable in 1D at temperature  $T = 0$  [25].

We now argue that the  $T = 0$  phase boundary between the PM phase and SSB phase is generically first order. The key observation is that the model at  $J > J_0$  has exponentially many ( $2^L - 1$  for PBC) nearly degenerate SSB ground states. This is because the number of ground states in SSB is generically polynomial in the number of charge sectors  $N_Q$  [46, 47], which grows exponentially in  $L$  (either OBC or PBC, see below Eq. (2)). This implies that at  $T = 0$ , the SSB phase has a fi-

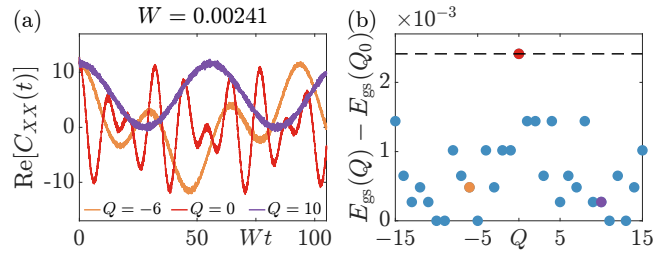


FIG. 4. (a) Autocorrelation  $C_{XX}(t) = \langle \psi_Q | \hat{S}_L^x(t) \hat{S}_L^x(0) | \psi_Q \rangle$  for PBC ground state  $|\psi_Q\rangle$  of three representative charge sectors  $Q$ , where  $J = \lambda = h = 1$ ,  $S = 5$  and  $L = 5$ . These states are highlighted in (b), which plots the energy levels in the PBC ground-state manifold (the dashed line indicates the bandwidth  $W = 0.00241$ ).

nite entropy density, while the PM phase has zero entropy density. More explicitly, as ED indicates, the PM ground state energy  $E_{\text{gs}}^{\text{sym}}$  and global SSB ground state energy  $E_{\text{gs}}(Q_0)$  are competing as  $E_{\text{gs}}^{\text{sym}} - E_{\text{gs}}(Q_0) = v_{\text{gs}}(J - J_0)L$  near  $J_0$ , with  $v_{\text{gs}} > 0$  (see SM [39]). Recall that for PBC, there are  $2^L - 1$  SSB ground states  $E_{\text{gs}}(Q)$  in the interval  $[E_{\text{gs}}(Q_0), E_{\text{gs}}(Q_0) + W]$ , while for OBC,  $E_{\text{gs}}(Q) - E_{\text{gs}}(Q_0) \approx D \left( \frac{Q-Q_0}{2^L} \right)^2$ . As temperature  $T = \beta^{-1} \rightarrow 0$ , we can ignore the other energy levels above the bulk gap, and approximate the Gibbs partition function as  $Z = e^{-\beta E_{\text{gs}}^{\text{sym}}} + \sum_Q e^{-\beta E_{\text{gs}}(Q)}$ . In the  $L \rightarrow \infty$  limit, regardless of the boundary condition, this yields a thermal entropy density (see SM [39])

$$\frac{S}{L} = \begin{cases} 0, & (J < J_T), \\ \ln 2, & (J \geq J_T), \end{cases} \quad J_T = J_0 - v_{\text{gs}}^{-1} T \ln 2. \quad (6)$$

Thus, at  $T = 0$ , the entropy density  $S/L$  jumps discontinuously by  $\ln 2$  at  $J = J_0$ , which enforces it to be a *first order* phase boundary between PM and SSB.

For 1D Gibbs states (with finite local Hilbert space) at temperatures  $T > 0$ , the Landau-Peierls instability from domain wall fluctuations (which are excitations above the bulk gap) restores the SSB and forbids any phase transition [48]. Nevertheless, Eq. (6) still implies a sharp crossover at  $J = J_T$  at low temperatures  $T > 0$ , as illustrated by the Fig. 3(a) phase diagram. Fig. 3(b) shows the color map of heat capacity  $C_v = T(\partial S/\partial T)$  from ED for  $L = 6$ , which is indeed peaked around  $J = J_T$ . The specific heat  $C_v/L$  as a function of  $J$  is smooth at high  $T$  [Fig. 3(c)], and shows a peak at low  $T$  [Fig. 3(d)]. The inset of Fig. 3(d) further shows that the entropy density  $S/L$  increases sharply by approximately  $\ln 2$  (sharper for the larger  $L$  calculated). Note that at  $J < J_0$ , the system crossovers from a more symmetric low-entropy regime to a less symmetric high-entropy regime as  $T$  increases, realizing a *Pomeranchuk effect* [49, 50].

*Glassy features.* The fact that the quantum breakdown condensate possesses exponentially many low-energy eigenstates and finite entropy density  $S/L = \ln 2$

suggests its analogy to a glass state. A glass state is hallmark by exponentially many equilibria and slow equilibration after a local perturbation, which are characters typically associated to quenched disorders. To examine whether the quantum breakdown condensate fulfills the defining features of a glass, we calculate the autocorrelation function  $C_{XX}(t) = \langle \phi_Q | \hat{S}_j^x(t) \hat{S}_j^x(0) | \psi_Q \rangle$  of local operator  $\hat{S}_j^x$  for the charge  $Q$  sector ground state  $|\psi_Q\rangle$  at  $J > J_0$ . Fig. 4 plots  $C_{XX}(t)$  at  $j = L$  for PBC in randomly selected charge sectors, all of which show non-decaying oscillations with periods on the order of  $2\pi/W$ , indicating glassy quantum dynamics. This is due to the fact that all local operators have a highly restricted connectivity only among the ground states of  $\mathcal{O}(1)$  number of charge sectors – for instance,  $\hat{S}_j^x$  only hops from charge sectors  $Q$  to  $Q \pm 2^{L-j}$ .

Moreover, there does not exist an off-diagonal long range order (ODLRO) [51] two-point function associated with the exponential  $U(1)$  SSB. The simplest symmetric two-point function formed by local order parameters is  $\langle \hat{S}_j^+(\hat{S}_{j+l}^-)^{2^l} \rangle$ , which vanishes identically as  $l \rightarrow \infty$ , since  $(\hat{S}_{j+l}^-)^{2^l} = 0$  for  $2^l > 2S$ . One can define a string order  $\langle \hat{S}_j^+(\prod_{k=1}^{l-1} \hat{S}_{j+k}^-)(\hat{S}_{j+l}^-)^2 \rangle$ , which however always scales (grows or decays) exponentially in  $l$  [25] and differs from the conventional ODLRO. Therefore, the order parameter  $\langle \hat{S}_j^+ \rangle$  is effectively short-range correlated, and is rather disordered as depicted in Fig. 1(b), making the exponential  $U(1)$  SSB drastically different from the SSB of conventional (including multipole) symmetries. These observations suggest that the quantum breakdown condensate can be viewed as a quantum glass, which interestingly arises from a disorder-free quantum Hamiltonian, in contrast to most known glass models.

*Discussion.* The quantum breakdown condensate from SSB of the exponential  $U(1)$  symmetry is exotic in its  $e^{cL}$  ( $c > 0$ ) number of SSB ground states in an  $\mathcal{O}(1)$  energy window from  $\mathcal{O}(e^{cL})$  number of charge sectors, and its absence of gapless Goldstone mode and ODLRO. This is different from the SSB of any other known symmetries, which at most have  $\mathcal{O}(L^p)$  ( $p \geq 0$ ) number of charge sectors. Note that the exponential  $\mathbb{Z}_N$  symmetry (with  $N$  independent of  $L$ ) is very different, having at most  $N$  SSB ground states [27–30]. The quantum breakdown condensate thus acts as a disorder-free quantum glass, which raises questions on its equilibration to Gibbs ensembles and its classification as a quantum phase of matter.

The exponentially many charge sectors closely resemble the Hilbert space fragmentation [7, 8, 52–54]. Each charge sector has no further fragmentation except for rare cases in PBC (see SM [39]). Moreover, a local operator can only sparsely connect an  $\mathcal{O}(1)$  number of charge sectors, leading to non-decaying autocorrelations (Fig. 4). This provides robustness against a class of errors in light of potentially applying the quantum breakdown condensate to store and process quantum information. In PBC,

the charge of the  $2^L - 1$  SSB ground states naturally maps to bit strings, making it possible to store information employing distinct ground states far separated in Hamming distance, for which the damage from a local perturbation is highly constrained and correctable. It would be interesting to explore experimental realizations of the spin quantum breakdown model in platforms such as Rydberg atoms.

*Acknowledgement.* We are especially grateful to David Huse for insightful discussions on phase transitions. We also thank Bo-Ting Chen, Steven Kivelson and Xiao-Liang Qi for helpful conversations. Z. H. is supported by a Simons Investigator award, the Simons Collaboration on Ultra-Quantum Matter, which is a grant from the Simons Foundation (651440). B. L. is supported by the National Science Foundation through Princeton University’s Materials Research Science and Engineering Center DMR-2011750, and the National Science Foundation under award DMR-2141966. Additional support is provided by the Gordon and Betty Moore Foundation through Grant GBMF8685 towards the Princeton theory program.

---

\* zhan@fas.harvard.edu

† biao@princeton.edu

- [1] J. McGreevy, Generalized symmetries in condensed matter, *Annual Review of Condensed Matter Physics* **14**, 57 (2023).
- [2] R. Luo, Q.-R. Wang, and Y.-N. Wang, Lecture notes on generalized symmetries and applications, *Physics Reports* **1065**, 1 (2024), lecture notes on generalized symmetries and applications.
- [3] E. J. Bergholtz and A. Karlhede, Quantum hall system in tao-thouless limit, *Phys. Rev. B* **77**, 155308 (2008).
- [4] M. Nakamura, Z.-Y. Wang, and E. J. Bergholtz, Exactly solvable fermion chain describing a  $\nu = 1/3$  fractional quantum hall state, *Phys. Rev. Lett.* **109**, 016401 (2012).
- [5] E. Lake, M. Hermele, and T. Senthil, Dipolar bose-hubbard model, *Phys. Rev. B* **106**, 064511 (2022).
- [6] M. Schulz, C. A. Hooley, R. Moessner, and F. Pollmann, Stark many-body localization, *Phys. Rev. Lett.* **122**, 040606 (2019).
- [7] V. Khemani, M. Hermele, and R. Nandkishore, Localization from hilbert space shattering: From theory to physical realizations, *Phys. Rev. B* **101**, 174204 (2020).
- [8] P. Sala, T. Rakovszky, R. Verresen, M. Knap, and F. Pollmann, Ergodicity breaking arising from hilbert space fragmentation in dipole-conserving hamiltonians, *Phys. Rev. X* **10**, 011047 (2020).
- [9] P. Gorantla, H. T. Lam, N. Seiberg, and S.-H. Shao, Global dipole symmetry, compact lifshitz theory, tensor gauge theory, and fractons, *Phys. Rev. B* **106**, 045112 (2022).
- [10] J.-K. Yuan, S. A. Chen, and P. Ye, Fractonic superfluids, *Phys. Rev. Res.* **2**, 023267 (2020).
- [11] S. A. Chen, J.-K. Yuan, and P. Ye, Fractonic superfluids. ii. condensing subdimensional particles, *Phys. Rev. Res.*

3, 013226 (2021).

[12] C. Stahl, E. Lake, and R. Nandkishore, Spontaneous breaking of multipole symmetries, *Phys. Rev. B* **105**, 155107 (2022).

[13] H.-X. Wang, S. A. Chen, and P. Ye, Fractonic superfluids. iii. hybridizing higher moments, *Phys. Rev. Res.* **7**, 033118 (2025).

[14] C. Chamon, Quantum glassiness in strongly correlated clean systems: An example of topological overprotection, *Phys. Rev. Lett.* **94**, 040402 (2005).

[15] J. Haah, Local stabilizer codes in three dimensions without string logical operators, *Phys. Rev. A* **83**, 042330 (2011).

[16] Y. You, T. Devakul, F. J. Burnell, and S. L. Sondhi, Subsystem symmetry protected topological order, *Phys. Rev. B* **98**, 035112 (2018).

[17] F. J. Burnell, T. Devakul, P. Gorantla, H. T. Lam, and S.-H. Shao, Anomaly inflow for subsystem symmetries, *Phys. Rev. B* **106**, 085113 (2022).

[18] T. Devakul, D. J. Williamson, and Y. You, Classification of subsystem symmetry-protected topological phases, *Phys. Rev. B* **98**, 235121 (2018).

[19] J. Distler, A. Karch, and A. Raz, Spontaneously broken subsystem symmetries, *Journal of High Energy Physics* **2022**, [https://doi.org/10.1007/JHEP03\(2022\)016](https://doi.org/10.1007/JHEP03(2022)016) (2022).

[20] N. E. Myerson-Jain, S. Yan, D. Weld, and C. Xu, Construction of fractal order and phase transition with rydberg atoms, *Phys. Rev. Lett.* **128**, 017601 (2022).

[21] N. E. Myerson-Jain, S. Liu, W. Ji, C. Xu, and S. Vijay, Pascal's triangle fractal symmetries, *Phys. Rev. Lett.* **128**, 115301 (2022).

[22] B. Lian, Quantum breakdown model: From many-body localization to chaos with scars, *Phys. Rev. B* **107**, 115171 (2023).

[23] B.-T. Chen, A. Prem, N. Regnault, and B. Lian, Quantum fragmentation in the extended quantum breakdown model, *Physical Review B* **110**, 10.1103/physrevb.110.165109 (2024).

[24] X. Liu and B. Lian, Two-dimensional quantum breakdown model with krylov subspace many-body localization, *Phys. Rev. B* **111**, 054302 (2025).

[25] Y.-M. Hu and B. Lian, Bosonic quantum breakdown hubbard model, *Phys. Rev. B* **112**, L100504 (2025).

[26] D. E. Kaplan and R. Rattazzi, Large field excursions and approximate discrete symmetries from a clockwork axion, *Physical Review D* **93**, 10.1103/physrevd.93.085007 (2016).

[27] Y. Hu and H. Watanabe, Spontaneous symmetry breaking without ground state degeneracy in generalized  $n$ -state clock model, *Phys. Rev. B* **107**, 195139 (2023).

[28] H. Watanabe, M. Cheng, and Y. Fuji, Ground state degeneracy on torus in a family of zn toric code, *Journal of Mathematical Physics* **64** (2023).

[29] G. Delfino, C. Chamon, and Y. You, 2d fractons from gauging exponential symmetries, arXiv preprint arXiv:2306.17121 (2023).

[30] J. H. Han, E. Lake, H. T. Lam, R. Verresen, and Y. You, Topological quantum chains protected by dipolar and other modulated symmetries, *Physical Review B* **109**, 125121 (2024).

[31] P. Sala, Y. You, J. Hauschild, and O. Motrunich, Exotic quantum liquids in bose-hubbard models with spatially modulated symmetries, *Phys. Rev. B* **109**, 014406 (2024).

[32] C. Wang, S. Balasubramanian, Y. Han, E. Lake, X. Chen, and Z.-C. Yang, *Exponentially slow thermalization in 1d fragmented dynamics* (2025), arXiv:2501.13930 [quant-ph].

[33] A. Rényi, Representations for real numbers and their ergodic properties, *Acta Math. Acad. Sci. Hungar.* **8**, 477 (1957).

[34] D. S. Rokhsar and S. A. Kivelson, Superconductivity and the quantum hard-core dimer gas, *Phys. Rev. Lett.* **61**, 2376 (1988).

[35] Z. Han and S. A. Kivelson, Models of interacting bosons with exact ground states: A unified approach, *Phys. Rev. B* **111**, 174520 (2025).

[36] E. N. Lorenz, Deterministic Nonperiodic Flow., *Journal of the Atmospheric Sciences* **20**, 130 (1963).

[37] J. Guckenheimer and R. F. Williams, Structural stability of lorenz attractors, *Publications Mathématiques de l'IHÉS* **50**, 59 (1979).

[38] W. Tucker, The lorenz attractor exists, *Comptes Rendus de l'Académie des Sciences-Series I-Mathematics* **328**, 1197 (1999).

[39] See Supplemental Material for details, which also includes references [? ?].

[40] N. Hatano and D. R. Nelson, Localization transitions in non-hermitian quantum mechanics, *Phys. Rev. Lett.* **77**, 570 (1996).

[41] S. Yao and Z. Wang, Edge states and topological invariants of non-hermitian systems, *Phys. Rev. Lett.* **121**, 086803 (2018).

[42] E. J. Bergholtz, J. C. Budich, and F. K. Kunst, Exceptional topology of non-hermitian systems, *Rev. Mod. Phys.* **93**, 015005 (2021).

[43] R. Lin, T. Tai, L. Li, and C. H. Lee, Topological non-hermitian skin effect, *Frontiers of Physics* **18**, 53605 (2023).

[44] N. D. Mermin and H. Wagner, Absence of ferromagnetism or antiferromagnetism in one- or two-dimensional isotropic heisenberg models, *Phys. Rev. Lett.* **17**, 1133 (1966).

[45] P. C. Hohenberg, Existence of long-range order in one and two dimensions, *Phys. Rev.* **158**, 383 (1967).

[46] H. Tasaki, Long-range order, “tower” of states, and symmetry breaking in lattice quantum systems, *Journal of Statistical Physics* **174**, 735 (2019).

[47] T. Koma and H. Tasaki, Symmetry breaking and finite-size effects in quantum many-body systems, *Journal of statistical physics* **76**, 745 (1994).

[48] D. Ruelle, *Statistical mechanics: Rigorous results* (World Scientific, 1969).

[49] I. Pomeranchuk, On the theory of liquid  $he^3$ , *Zhur. Eksppl'. i Teoret. Fiz.* **20** (1950).

[50] R. C. Richardson, The pomeranchuk effect, *Rev. Mod. Phys.* **69**, 683 (1997).

[51] C. N. Yang, Concept of off-diagonal long-range order and the quantum phases of liquid  $he$  and of superconductors, *Rev. Mod. Phys.* **34**, 694 (1962).

[52] S. Moudgalya, A. Prem, R. Nandkishore, N. Regnault, and B. A. Bernevig, Thermalization and its absence within krylov subspaces of a constrained hamiltonian, in *Memorial Volume for Shoucheng Zhang* (World Scientific, 2022) pp. 147–209.

[53] S. Moudgalya and O. I. Motrunich, Hilbert space fragmentation and commutant algebras, *Phys. Rev. X* **12**, 011050 (2022).

[54] S. Moudgalya, B. A. Bernevig, and N. Regnault, Quantum many-body scars and hilbert space fragmentation: a review of exact results, [Reports on Progress in Physics](#) **85**, 086501 (2022).

# Supplemental Material: Quantum Breakdown Condensate as a Disorder-Free Quantum Glass

Yu-Min Hu,<sup>1</sup> Zhaoyu Han,<sup>2,\*</sup> and Biao Lian<sup>3,†</sup>

<sup>1</sup>Max Planck Institute for the Physics of Complex Systems, Nöthnitzer Straße 38, 01187 Dresden, Germany

<sup>2</sup>Department of Physics, Harvard University, Cambridge, Massachusetts 02138, USA

<sup>3</sup>Department of Physics, Princeton University, Princeton, New Jersey 08544, USA

## I. ED ENERGY SPECTRA FOR OTHER SPINS $S$

In this section, we present additional ED numerical results to show that the physics discussed in the main text generally occurs for many other spin  $S$  values. Fig. S1 presents the ED energy spectrum under periodic boundary conditions (PBC) for different spin  $S$  and different values of  $\lambda$ . For large enough  $J/h$  (here  $J/h = 1$ ), the system will enter the spontaneous-symmetry-breaking (SSB) phase, in which we find the ground states from each PBC charge sector are almost degenerate. The low-energy spectra in Fig. S1 clearly demonstrate that, the total bandwidth of the ground-state manifold, defined as  $W = E_{2^L-1} - E_1 = \max_Q[E_{\text{gs}}(Q)] - \min_Q[E_{\text{gs}}(Q)]$  with  $E_n$  being the  $n$ -th energy eigenvalue from low to high among all charge sectors  $Q$ , decreases as  $S$  increases [as summarized by Fig. 2(h) of the main text]. Furthermore, we note that the ED spectra are qualitatively similar for different choices of  $\lambda$ . These results suggest that the SSB physics of the exponential U(1) symmetry is independent of the concrete form of symmetric on-site interactions.

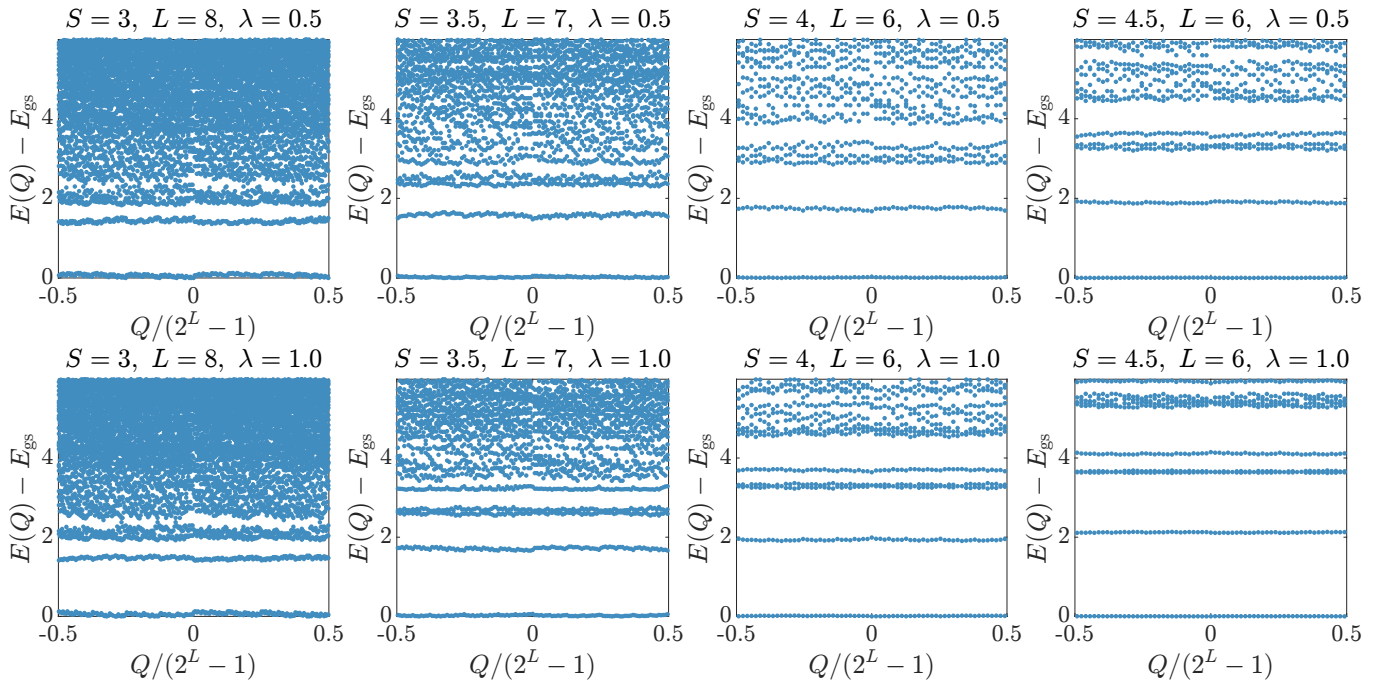


FIG. S1. The PBC ED spectra of the model with respect to charge sector  $Q$ , for  $J = h = 1$  (in the SSB phase) and different choices of  $S$ ,  $L$ , and  $\lambda$  as labeled in each panel.

\* zhan@fas.harvard.edu

† biao@princeton.edu

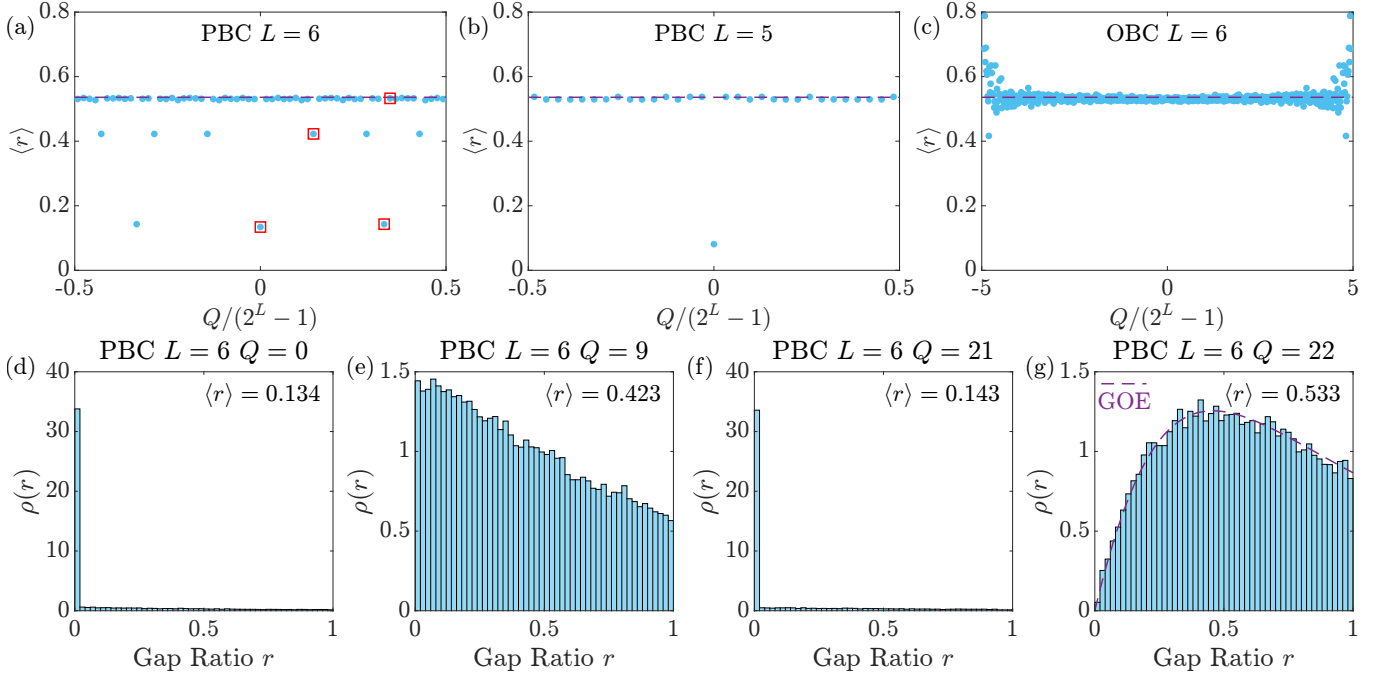


FIG. S2. In all plots, we fix the parameters  $S = 5$  and  $J = h = \lambda = 1$ . (a-c) The mean values of gap ratios for different charge sectors, with the boundary conditions and the system size shown in each plot. The dashed line is the theoretical value 0.536 of the random Gaussian orthogonal ensemble. (d-g) The gap-ratio distribution for four representative PBC charge sectors marked as red squares in (a). The dashed line in (g) represents the Gaussian orthogonal ensemble (GOE).

## II. LEVEL STATISTICS IN EACH CHARGE SECTOR

We now investigate the level spacing statistics for the spin quantum breakdown model. Without loss of generality, we focus on the parameters  $S = 5$  and  $J = h = \lambda = 1$ . These parameters are the same as in the Figs. 2(c) and 2(d) of the main text. In each exponential charge sector  $Q$ , we have many eigenenergies  $E_1^{(Q)} \leq \dots \leq E_{d_Q}^{(Q)}$  in increasing order, where  $d_Q$  is the Hilbert space dimension of the charge sector  $Q$  for a fixed system size. In each exponential charge sector  $Q$ , we can calculate the gap ratio [1]

$$r_n = \frac{\min(\Delta_n, \Delta_{n+1})}{\max(\Delta_n, \Delta_{n+1})} \quad (\text{S1})$$

where  $\Delta_n = E_{n+1}^{(Q)} - E_n^{(Q)}$  is the gap between two neighboring energies.

Figs. S2 (a-c) shows the mean gap ratio [1, 2]  $\langle r \rangle = \frac{1}{d_Q-2} \sum_{n=1}^{d_Q-2} r_n$  for each  $Q$  sector with different boundary conditions and system sizes. These numerical results indicate that, regardless of boundary conditions and system sizes, most charge sectors have a mean gap ratio  $\langle r \rangle$  close to 0.536, exhibiting a gap ratio distribution like Fig. S2(g) which is consistent with the Gaussian orthogonal ensemble (GOE) [2]. This reveals that most charge sectors are chaotic. There is no additional symmetry that could induce further block diagonalization within these charge sectors.

However, as shown in Figs. S2 (a) and (b), there are a few PBC charge sectors whose mean gap ratio significantly deviates from the GOE value 0.536. Three typical gap ratio distributions shown in Fig. S2(d-f) demonstrate that the energy spectrum of these anomalous PBC charge sectors has many degenerate eigenvalues, which implies the existence of additional symmetry besides the exponential symmetry. For comparison, such anomalous charge sectors are not observed under an open boundary condition [see Fig. S2(c)], where the deviation of  $\langle r \rangle$  near  $Q/(2^L - 1) \approx \pm 5$  merely comes from the smallness of the Hilbert space dimension for these OBC charge sectors.

The difference between the boundary conditions indicates that the translation symmetry under periodic boundary conditions may play a role in shaping the level statistics in these anomalous PBC charge sectors. In the rest of this section, we focus on the PBC and investigate the role of translation symmetry. As discussed in the main text, the PBC exponential charge operator  $\hat{Q} = \sum_{j=1}^L 2^{L-j} \hat{S}_j^z \bmod (2^L - 1)$  and the PBC translation symmetry  $\hat{T}$  have a commutation relation  $\hat{T} \hat{Q} \hat{T}^{-1} = 2\hat{Q} \bmod (2^L - 1)$ . Generally,  $\hat{T}$  transfers a state  $|\psi_{2Q}\rangle$  in the  $2Q$  charge sector

satisfying  $\hat{Q}|\psi_{2Q}\rangle = 2Q|\psi_{2Q}\rangle$  into another state  $\hat{T}|\psi_{2Q}\rangle$  in the  $Q$  charge sector. Here, the eigenvalue of  $\hat{Q}$  is defined mod  $2^L - 1$ . This can be easily proved by the observation that  $\hat{Q}\hat{T}|\psi_{2Q}\rangle = \frac{1}{2}\hat{T}\hat{Q}|\psi_{2Q}\rangle = Q\hat{T}|\psi_{2Q}\rangle$ . Therefore, a generic PBC charge sector with the exponential charge  $Q$  is likely not invariant under the one-time action of the translation symmetry.

Nevertheless, the above analysis does not exclude the possibility that for some specific charge sector  $Q$  and for an integer  $m \in \{1, 2, \dots, L-1\}$ <sup>1</sup>, the relation  $Q = 2^m Q \bmod 2^L - 1$  can be satisfied. In such a case, the  $Q$  sector is invariant under the action of  $\hat{T}^m$ . As a result, the  $m$ -step translation operation  $\hat{T}^m$  can further block diagonalize the  $Q$  sector into different Krylov subspaces labeled by different momenta. We remark that these Krylov subspaces are reminiscent of quantum fragmentation, since a general root state with a definite momentum does not have a product-state structure in the computational basis.

A trivial example is  $Q = 0$  and  $m = 1$  for an arbitrary system size  $L$ , as observed in Fig. S2(a) and (b). We also note that Fig. S2(a) also indicates several anomalous charge sectors with  $Q \neq 0$  for  $L = 6$ . These charge sectors can be divided into two groups: (1)  $Q = \pm 9, \pm 18, \pm 27$  and  $m = 3$ , as exemplified in Fig. S2(e); (2)  $Q = \pm 21$  and  $m = 2$ , as exemplified in Fig. S2(f).

We have revealed that these anomalous charged sectors have an additional symmetry as some subgroups of the translation symmetry. With this intuition in mind, we now discuss the general approach for identifying these anomalous charged sectors in a generic system. With the system size  $L$  and an integer  $m \in \{1, 2, 3, \dots, L-1\}$ , we first define the greatest common divisor (gcd) between  $m$  and  $L$ , i.e.,  $g = \gcd(m, L)$ . Then the equation  $Q = 2^m Q \bmod 2^L - 1$  is solved by  $Q = 0 \bmod \frac{2^L - 1}{2^g - 1}$ <sup>2</sup>. There are  $2^g - 1$  solutions:  $Q = \frac{2^L - 1}{2^g - 1}k$  with  $k = 0, 1, \dots, 2^g - 2$ . Specifically, when  $g = \gcd(m, L) = 1$ , the only solution is  $Q = 0$ . As a benchmark, we apply this general result to Fig. S2(a) and (b). In Fig. S2(a), we have  $L = 6$ . First,  $\gcd(1, 6) = \gcd(5, 6) = 0$  leads to the  $Q = 0$  sector; second,  $\gcd(2, 6) = \gcd(4, 6) = 2$  results in three sectors  $Q = 0, 21, 42$ ; last,  $\gcd(3, 6) = 3$  provides seven sectors  $Q = 0, 9, 18, 27, 36, 45, 54$ . In Fig. S2(b), we have  $L = 5$  and therefore  $\gcd(1, 5) = \gcd(2, 5) = \gcd(3, 5) = \gcd(4, 5) = 1$ . The only solution in this case is  $Q = 0$ , as observed in Fig. S2(b).

The above solutions of the anomalous charge sectors have an intuitive picture. As the exponential charge  $Q$  is defined up to multiples of  $2^L - 1$ , each  $Q$  can be uniquely mapped to a length- $L$  bit string, which can be viewed as a root state. For example, when  $L = 6$ ,  $Q = 0, 9, 21$  can be mapped into 000000, 001001, and 010101, respectively. Therefore,  $g = \gcd(m, L)$ , as a factor of  $L$ , indicates the sub- $L$  periodicity of these bit strings with a periodic boundary condition. This also indicates that there exists only a small number of anomalous charge sectors when the system size  $L$  is a composite number. These anomalous sectors have additional symmetries originating from the subgroups of translation. In contrast, the bit strings for most PBC charge sectors do not have such a periodicity, which indicates a chaotic behavior in their level statistics.

### III. GROUND STATE PHASE TRANSITION AND FINITE-TEMPERATURE PHASE DIAGRAM

In this section, we provide additional data for the zero-temperature phase transition and finite-temperature crossover, for which the ED numerical results as presented in Fig. S3 and Fig. S4.

The zero-temperature first-order phase transition between the two distinct types of ground states is revealed by a level crossing between the paramagnetic state and the SSB manifold, as shown in Figs. S3(a), S3(e), and S4(a) for PBC. This level crossing is further manifested by discontinuous jumps in the derivative of the ground-state energy with respect to the breakdown interaction strength, as displayed in Figs. S3(b), S3(f), and S4(c). A similar first-order phase transition is also observed in the low-energy spectrum of systems under open boundary conditions (OBC), as shown in Figs. S4(b) and S4(c). We remark that the PBC phase transition points [Figs. S3(b) and S3(f)] are independent of the system size  $L$ . In contrast, the OBC phase transition points [Fig. S4(c)] exhibit a finite-size effect, which converge to the PBC transition points as the system size  $L$  increases.

The zero-temperature phase transition from PM to the SSB quantum breakdown condensate is expected to remain a sharp crossover in the low-temperature regime. Due to the sharp difference in ground-state degeneracy between two phases, the zero-temperature phase transition and finite-temperature crossover can be estimated by entropy considerations.

<sup>1</sup>  $m = 0$  and  $m = L$  are trivial since  $\hat{T}^0 = \hat{T}^L = I$  is the identity.

<sup>2</sup> This solution can be proved as follows. First, the original equation  $Q = 2^m Q \bmod 2^L - 1$  can also be expressed as  $(2^m - 1)Q = 0 \bmod 2^L - 1$ . We can define an integer  $g_0 = \gcd(2^m - 1, 2^L - 1)$ , such that  $(2^m - 1)Q = 0 \bmod 2^L - 1$  is transformed into  $\frac{2^m - 1}{g_0}Q = 0 \bmod \frac{2^L - 1}{g_0}$ . Since  $\gcd(\frac{2^m - 1}{g_0}, \frac{2^L - 1}{g_0}) = 1$ , we conclude that  $Q = 0 \bmod \frac{2^L - 1}{g_0}$ . Now we need to prove that  $g_0 = \gcd(2^m - 1, 2^L - 1) = 2^{\gcd(m, L)} - 1 = 2^g - 1$ . On the one hand,  $g = \gcd(m, L)$  indicates that  $m/g$  and  $L/g$  are integers. In this sense,  $2^m - 1 = (2^g)^{m/g} - 1 = (2^g - 1)[1 + 2^g + (2^g)^2 + \dots + (2^g)^{m/g-1}]$  and  $2^L - 1 = (2^g)^{L/g} - 1 = (2^g - 1)[1 + 2^g + (2^g)^2 + \dots + (2^g)^{L/g-1}]$ . This tells that  $2^g - 1$  is a common divisor of  $2^m - 1$  and  $2^L - 1$ . On the other hand,  $\gcd(2^m - 1, 2^L - 1) = \gcd(2^m - 1, 2^L - 1 - 2^{L-m}(2^m - 1)) = \gcd(2^m - 1, 2^{L-m} - 1)$ . This relation further leads to  $\gcd(2^m - 1, 2^L - 1) = \gcd(2^m - 1, 2^L \bmod m - 1)$ . The change of exponents in these equations is equivalent to the Euclidean algorithm in calculating  $\gcd(m, L)$ . As a result, we prove that  $\gcd(2^m - 1, 2^L - 1) = \gcd(2^{\gcd(m, L)} - 1, 2^0 - 1) = 2^{\gcd(m, L)} - 1$ .

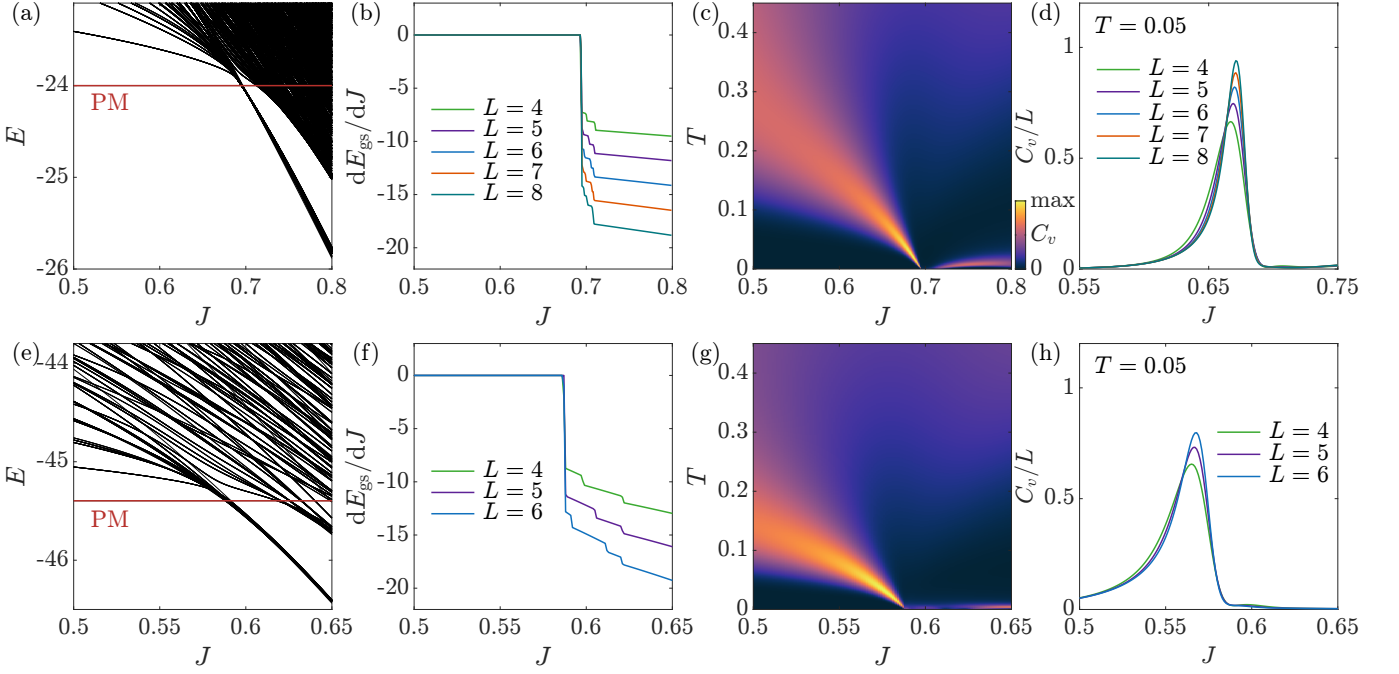


FIG. S3. (a,e) The PBC low-energy ED spectrum  $E$  with respect to the breakdown interaction  $J$ . The red line with label PM represents the energy of the paramagnetic (PM) state. A clear level crossing between PM and  $2^L - 1$  SSB ground states indicates a first order phase transition. (b,f) The ground-state energy derivative  $dE_{\text{gs}}/dJ$ . (c,g) The finite-temperature colormap representing the heat capacity  $C_v$ , which agrees with the expected phase diagram in the main text. (d,h) The specific heat  $C_v/L$  with  $T = 0.05$  for different system sizes. In (a-d), we fix  $S = 3$ ,  $\lambda = h = 1$ . We also fix  $L = 8$  for (a) and (c). In (e-h), we fix  $S = 5$ ,  $\lambda = 0.5$ ,  $h = 1$ . We also fix  $L = 6$  for (e) and (g). We take PBC in all plots here.

Subsequently, we present more details of this low temperature entropy calculation. For  $J$  near the SSB phase transition point  $J_0$ , the low energy competing states are the symmetric PM ground state with energy  $E_{\text{gs}}^{\text{sym}}$ , and the SSB ground state in each charge sector  $Q$  with energy  $E_{\text{gs}}(Q)$ . Assume the state  $E_{\text{gs}}(Q_0)$  in charge sector  $Q_0$  is the lowest among all the SSB ground states. The ED results indicate that [Figs. S3(a) and S3(e)]

$$E_{\text{gs}}^{\text{sym}} - E_{\text{gs}}(Q_0) = v_{\text{gs}}(J - J_0)L, \quad (v_{\text{gs}} > 0) \quad (\text{S2})$$

which effectively describes the level crossing at  $J = J_0$ . At low temperatures  $T = 1/\beta$  (we set  $k_B = 1$ ), to the leading order we ignore all the states above the bulk gap  $\Delta$ , and obtain an approximate partition function given by keeping only the above competing ground states:

$$Z = e^{-\beta E_{\text{gs}}^{\text{sym}}} + \sum_Q e^{-\beta E_{\text{gs}}(Q)}. \quad (\text{S3})$$

(i) For PBC, there are  $2^L - 1$  charge  $Q$  sectors, of which the ground state energies  $E_{\text{gs}}(Q)$  lie in the energy interval  $[E_{\text{gs}}(Q_0), E_{\text{gs}}(Q_0) + W]$ , where  $W$  is of order one ( $W < \Delta$ ). If we approximately regard  $E_{\text{gs}}(Q)$  as uniformly distributed in the bandwidth  $W$ , we find

$$\begin{aligned} Z &\approx e^{-\beta E_{\text{gs}}^{\text{sym}}} + (2^L - 1)e^{-\beta E_{\text{gs}}(Q_0)} \int_0^W dE \frac{e^{-\beta E}}{W} \\ &\approx e^{-\beta E_{\text{gs}}(Q_0)} \left[ e^{-\beta v_{\text{gs}}(J - J_0)L} + 2^L \frac{1 - e^{-\beta W}}{\beta W} \right]. \end{aligned} \quad (\text{S4})$$

(ii) For OBC, in ED (and by the analytical edge mode argument in the main text) we approximately find  $E_{\text{gs}}(Q) -$

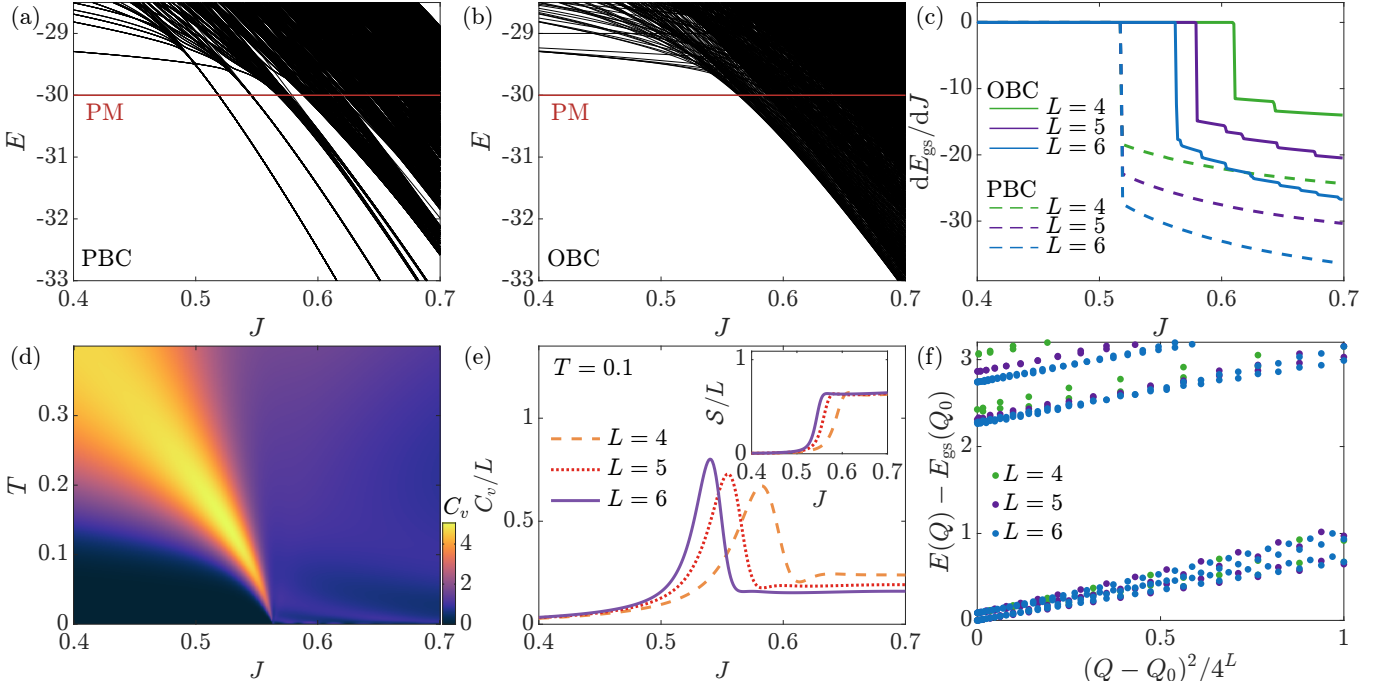


FIG. S4. The ED spectra and thermal quantities under different boundary conditions for  $S = 5, \lambda = h = 1$  (the parameters of the main example in the main text). These parameters are the same as Fig. 2 of the main text. (a) The low-energy PBC spectrum  $E$  with respect to the breakdown interaction  $J$  for the system size  $L = 6$ . (b) The low-energy OBC spectrum  $E$  with respect to the breakdown interaction  $J$  for the system size  $L = 6$ . The red lines in (a) and (b), which are labelled by PM, represent the energy of the paramagnetic state. (c) The ground-state energy derivative  $dE/dJ$  for PBC (dashed lines labelled by the system size  $L$ ) and OBC (solid lines labeled by the system size  $L$ ) systems. (d) The heat capacity  $C_v$  for  $L = 6$  under open boundary conditions. (e) The specific heat  $C_v/L$  and the entropy density  $S/L$  (inset) at  $T = 0.1$  for different system sizes  $L$  under open boundary conditions. (f) The low-energy OBC spectrum for  $L = 6$  and  $J = 1$ .

$E_{\text{gs}}(Q_0) \approx D \left( \frac{Q-Q_0}{2^L} \right)^2$ . An example can be found in Fig. S4(f) [see also Fig. 2(d) of the main text]. Thus,

$$\begin{aligned} Z &\approx e^{-\beta E_{\text{gs}}^{\text{sym}}} + e^{-\beta E_{\text{gs}}(Q_0)} \sum_Q e^{-D \left( \frac{Q-Q_0}{2^L} \right)^2} \\ &\approx e^{-\beta E_{\text{gs}}(Q_0)} \left[ e^{-\beta v_{\text{gs}}(J-J_0)L} + 2^L \int_{-\infty}^{\infty} dx e^{-\beta D x^2} \right] \\ &= e^{-\beta E_{\text{gs}}(Q_0)} \left[ e^{-\beta v_{\text{gs}}(J-J_0)L} + 2^L \sqrt{\frac{\pi}{\beta D}} \right], \end{aligned} \quad (\text{S5})$$

where we have defined  $x = \frac{Q-Q_0}{2^L}$  in the second line.

It is then easy to calculate the thermal entropy  $\mathcal{S} = \ln Z - \beta \partial_\beta \ln Z$ . Interestingly, in the  $L \rightarrow \infty$  limit, the entropy density  $\mathcal{S}/L$  for both PBC and OBC takes the same form:

$$\frac{\mathcal{S}}{L} = \begin{cases} 0, & (J < J_T) \\ \ln 2, & (J \geq J_T) \end{cases}, \quad J_T = J_T = J_0 - v_{\text{gs}}^{-1} T \ln 2. \quad (\text{S6})$$

This result further supports that the difference between PBC and OBC is only on the boundaries, not in the bulk, as is expected for physical systems with local Hamiltonians. This implies that the crossover boundary  $J_T$  at finite temperature is on the  $J < J_0$  side, in agreement with our ED calculations.

According to the Landau-Peierls instability [3], at finite temperature  $T > 0$ , thermal fluctuations from proliferating domain walls, which are excitations above the bulk gap, will always restore the SSB and forbids any phase transitions. Therefore, we expect  $J = J_T$  to be a crossover boundary at  $T > 0$ .

The finite-temperature colormaps of heat capacity shown in Figs. S3(c), S3(g), and S4(d) resemble that in Fig. 3(b) of the main text, indicating a finite-temperature crossover realizing a Pomeranchuk effect. Near the crossover

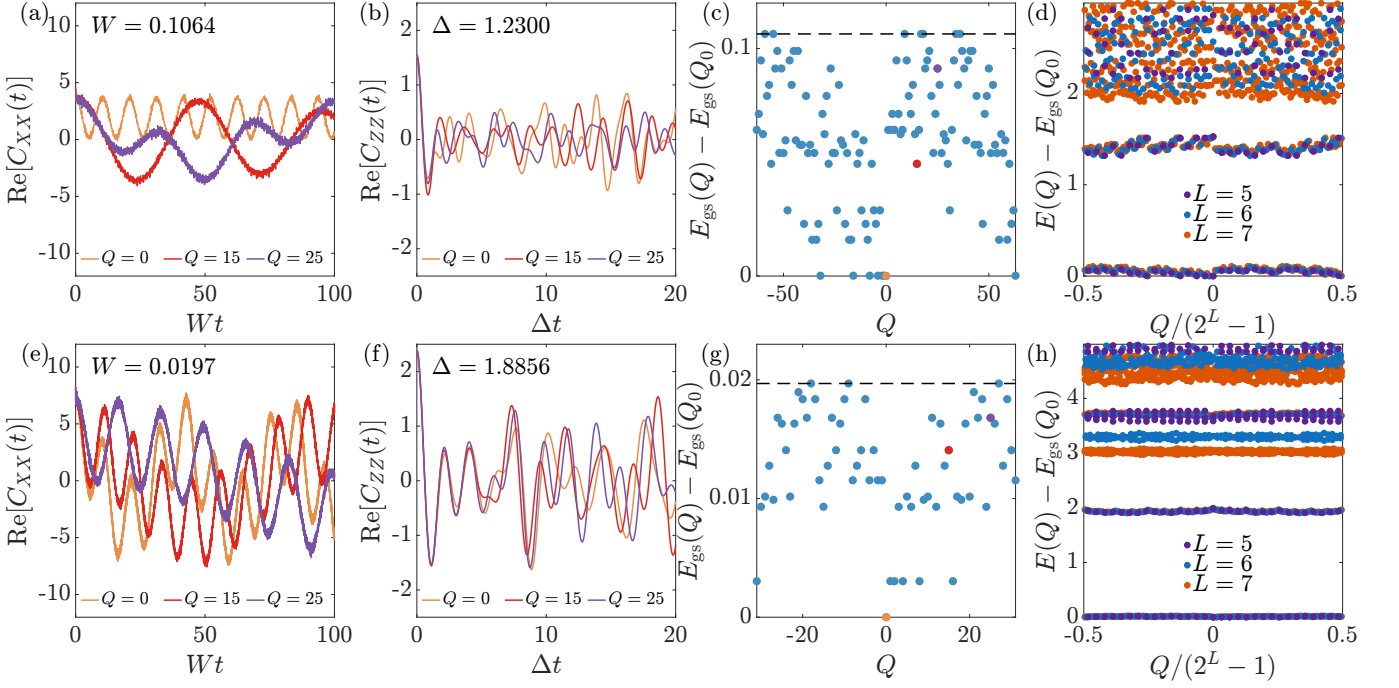


FIG. S5. (a,e) The autocorrelation functions  $C_{XX}(t)$  calculated by ED. (b,f) The autocorrelation functions  $C_{ZZ}(t)$  calculated by ED. (c,g) The energy distribution of the PBC ground-state manifold, where the dashed line labels the bandwidth  $W$ . (d,h) The low-energy PBC spectra for different system sizes. We set  $S = 3, \lambda = 0.5, h = J = 1$  in (a-d) and  $L = 7$  in (a-c). Similarly, the parameters in (e-h) are  $S = 4, \lambda = 1.0, h = J = 1$ , with  $L = 6$  in (e-g).

boundary, the specific heat  $C_v/L$  shows a sharp peak [Figs. S3(d), S3(h), and S4(e)], which tends to sharpen for the larger system size  $L$  calculated, indicating a sharp crossover at low temperatures. The finite-size effect of the zero-temperature phase transition for OBC systems is also observed for the finite-temperature crossover. As shown in Fig. S4(e), the locations of specific heat peaks and entropy jumps move monotonically with respect to the system size  $L$ , showing a considerable finite size effect.

We note that while Fig. S4 is calculated with parameters the same as that in Fig. 3 of the main text, Fig. S3 presents two different sets of parameters. These results demonstrate that the zero-temperature first-order transition and finite-temperature crossover remain robust against variations of the microscopic model details.

#### IV. ADDITIONAL DATA ON GLASSY DYNAMICS

In this section, we further investigate the glassy dynamics. For a given spin chain with PBC, we study the autocorrelation functions with the initial state  $|\psi_Q\rangle$  being the ground state of a specific charge sector  $Q$ . Then we evaluate the autocorrelation function

$$C_{XX}(t) = \langle \psi_Q | \hat{S}_L^x(t) \hat{S}_L^x(0) | \psi_Q \rangle, \quad C_{ZZ}(t) = \langle \psi_Q | \hat{S}_L^z(t) \hat{S}_L^z(0) | \psi_Q \rangle - \langle \psi_Q | \hat{S}_L^z(t) | \psi_Q \rangle \langle \psi_Q | \hat{S}_L^z(0) | \psi_Q \rangle. \quad (\text{S7})$$

Here, the time evolution of an operator  $\hat{O}$  is given by  $\hat{O}(t) = e^{i\hat{H}t} \hat{Q} e^{-i\hat{H}t}$ . Without loss of generality for PBC, we focus on the spin operators on the last site  $j = L$ . The numerical results for the autocorrelation functions on other sites exhibit similar behaviors. On one hand, since  $\hat{S}_L^x$  does not commute with the exponential symmetry  $\hat{Q} = \sum_{j=1}^L 2^{L-j} \hat{S}_j^z \bmod 2\pi$ , we have  $\langle \psi_Q | \hat{S}_L^x(t) | \psi_Q \rangle = 0$ . On the other hand,  $\langle \psi_Q | \hat{S}_L^z(t) | \psi_Q \rangle = \langle \psi_Q | \hat{S}_L^z(0) | \psi_Q \rangle \neq 0$ .

Numerically, we perform the exact diagonalization for the Hamiltonian  $\hat{H}_Q$  restricted to the charge sector  $Q$ , whose eigenvalues (from low to high) and eigenstates are denoted as  $E_n^{(Q)}$  and  $|\phi_n^{(Q)}\rangle$ . Note that the above initial state  $|\psi_Q\rangle \equiv |\psi_1^{(Q)}\rangle$  is chosen as the ground state in the charge sector  $Q$ . With this notation, we find that

$$C_{XX}(t) = \sum_{Q'} \sum_{n_{Q'}} e^{i(E_1^{(Q)} - E_{n_{Q'}}^{(Q')})t} |\langle \phi_{n_{Q'}}^{(Q')} | \hat{S}_L^x | \psi_Q \rangle|^2, \quad (\text{S8})$$

where  $Q'$  is the label of the charge sectors that are connected to the sector  $Q$  by applying  $\hat{S}_L^x$ . As shown in Fig. S1, in the PBC system with a large breakdown interaction, the ground states of all the charge sectors are nearly degenerate within the ground state manifold bandwidth  $W$ . In other words,  $E_1^{(Q)} - E_1^{(Q')}$  is on the order of  $W$ . On the contrary,  $E_1^{(Q)} - E_{n_{Q'}}^{(Q')}$  with  $n_{Q'} > 1$  is generally greater than the bulk excitation gap  $\Delta$ . For relatively large spin  $S$  where  $\Delta \gg W$ , we have  $|E_1^{(Q)} - E_1^{(Q')}| \ll |E_1^{(Q)} - E_{n_{Q'}}^{(Q')}|$ . As a result, the contribution of excited states in the charge sector  $Q'$  to  $C_{XX}(t)$  oscillates very fast and destructively. Therefore, the leading contribution to  $C_{XX}(t)$  comes from the dynamics within the ground-state manifold, which leads to

$$C_{XX}(t) \approx \sum_{Q'} e^{i(E_1^{(Q)} - E_1^{(Q')})t} |\langle \psi_{Q'} | \hat{S}_L^x | \psi_Q \rangle|^2. \quad (\text{S9})$$

This autocorrelation has a slow oscillation timescale  $\tau_X \propto 1/W$ . Such an expectation is supported by the ED numerical results shown in Fig. S5(a,e).

As for the autocorrelation of  $S_L^z$ , we note that applying  $\hat{S}_L^z$  on  $|\psi_Q\rangle$  does not alter the charge sector  $Q$ . Therefore, we can find that

$$\begin{aligned} C_{ZZ}(t) &= \sum_{n_Q} e^{i(E_1^{(Q)} - E_{n_Q}^{(Q)})t} |\langle \phi_{n_Q}^{(Q)} | \hat{S}_L^z | \psi_Q \rangle|^2 - |\langle \psi_Q | \hat{S}_L^z | \psi_Q \rangle|^2 \\ &= \sum_{n_Q \geq 2} e^{i(E_1^{(Q)} - E_{n_Q}^{(Q)})t} |\langle \phi_{n_Q}^{(Q)} | \hat{S}_L^z | \psi_Q \rangle|^2. \end{aligned} \quad (\text{S10})$$

Since  $E_{n_Q}^{(Q)} - E_1^{(Q)} > \Delta$  and the distribution of  $E_{n_Q}^{(Q)}$  with  $n_Q \geq 2$  depends on the system size [Figs. S5(d,h)], we expect fast dynamics for  $C_{ZZ}(t)$  (subject to finite size effect), which is supported by the ED numerical results in Fig. S5(b,f).

---

[S1] V. Oganesyan and D. A. Huse, Localization of interacting fermions at high temperature, *Phys. Rev. B* **75**, 155111 (2007).  
 [S2] Y. Y. Atas, E. Bogomolny, O. Giraud, and G. Roux, Distribution of the ratio of consecutive level spacings in random matrix ensembles, *Phys. Rev. Lett.* **110**, 084101 (2013).  
 [S3] D. Ruelle, *Statistical mechanics: Rigorous results* (World Scientific, 1969).